Hyperspectral image analysis of Aguas Teñidas, Magdalena, Sotiel and Majada deposits: towards a drill-core scan in the Iberian Pyrite Belt

Pedro S.T. Mendes, Pierre Barnabé, Eric Pirard
Minerals Engineering, Materials and Environment (GeMMe), Université de Liège, Belgium

Juan Manuel Pons, Juan Carlos V. Vasquez
Minas de Aguas Teñidas SAU (MATSA), Spain

Carlos G. Piña
DMT GmbH & Co. KG

Abstract. Analysis of VNIR-SWIR hyperspectral images is presented to assist the development of a multi-sensor scanning system for Iberian Pyrite Belt Cu-Zn-Pb projects. Fisher Linear Discriminant and Linear Support Vector Classifier were used for supervised classification after pre-processing, spectral plotting and construction of false color composites. Validation is given by mean accuracy of confusion matrices for different scenarios considering parameters of practical applications in industrial settings. Interpretation indicates a different performance for shale and volcanic-hosted deposits. The results demonstrate the power of machine learning algorithms and hyperspectral databases applied to an automated technique to assist the traditional logging. Combined to other sensors, the methodology should be adapted to a drill-core scan delivering cost-effective and time-saving outcomes.

1 Introduction

Hyperspectral imaging (HSI) concentrates on the diversity of spectral properties inherent to each material. In other words, the light that is emitted or reflected and its variation along narrow wavelength ranges. The link between these physical properties and earth sciences has emerged to map geological parameter in different scales (Hunt 1977; Goetz et al. 1985).

The logging of drill cores has been carried out by geologists using visual inspection. Despite providing important basic information, the technique has demonstrated to be subjective. In this work, the potential of machine learning algorithms combined to HSI is evaluated as an automated logging tool by testing different supervised classification strategies. The chosen method is considered supervised because it is assisted by a previous user knowledge (Han et al. 2012).

This research aims to contribute to the classification of rocks in the Iberian Pyrite Belt volcano-sedimentary complex in a consistent manner. The work comprises a fundamental step of ANCORELOG, an EIT Raw Materials-funded project working on the development of a multi-sensor analytical drill-core scan. Finally, the new prototype will extend the functionality of DMT CoreScan System, improving utilization of ore bodies from exploration to mineral processing (Lamberg 2012).

Predictions of performance in practical applications are evaluated for the following Cu-Zn-Pb ventures: Aguas Teñidas and Patata Frita (ATE); Magdalena (MAG); Sotiel and Elvira (SOT); also, the drilling campaign of Majada (MAD). The underground mines and surface exploration areas associated to each deposit are illustrated in Fig. 1.

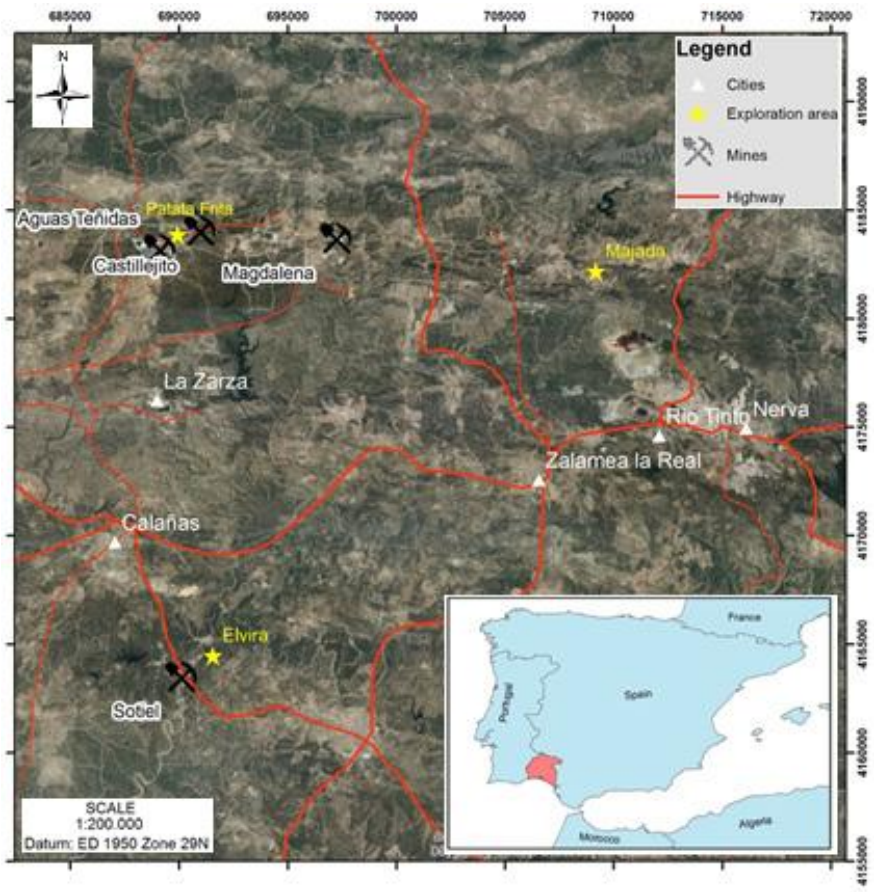

Figure 1. Study area (Mendes 2018).

2 Methodology

2.1 Sampling

Characterization was carried out through visual drill core logging and mine front description. The divergence between two metallonegetic environments was considered (Martin-Izard et al. 2016): Shale hosted deposits of Type 1 (SOT and MAD) and Volcanogenic Massive Sulphides (VMS) of Type 2 (ATE and MAG), where extrusives dominate.

In total 40 samples were collected following a systematic protocol to ensure representativeness of lithology, texture, alteration degree and metal grade.

Chemical assays of valuable metals and penalty elements from 10 mineralized samples with cupriferous stockwork and massive cupriferous/polymetallic ore were given by ICP-OES. Main minerals are chalcopyrite, sphalerite and galena.

2.2 Image acquisition and pre-processing

The images were acquired using a Specim SWIR camera and a VNIR, which is composed by a Specim ImSpectorV10E spectrograph and a Photonfocus MV1-D1312ie sensor (Fig. 2). Both cameras are placed horizontally over a 2.5 m frame to detect the reflected light from the samples in a line pointing the conveyor belt through mirrors (Barnabé et al. 2015). The approximately 350 mm line in the field of view is placed at the focuses of extruded elliptical reflectors so it is illuminated with constant light by halogen lamps, that are situated at the other focuses.

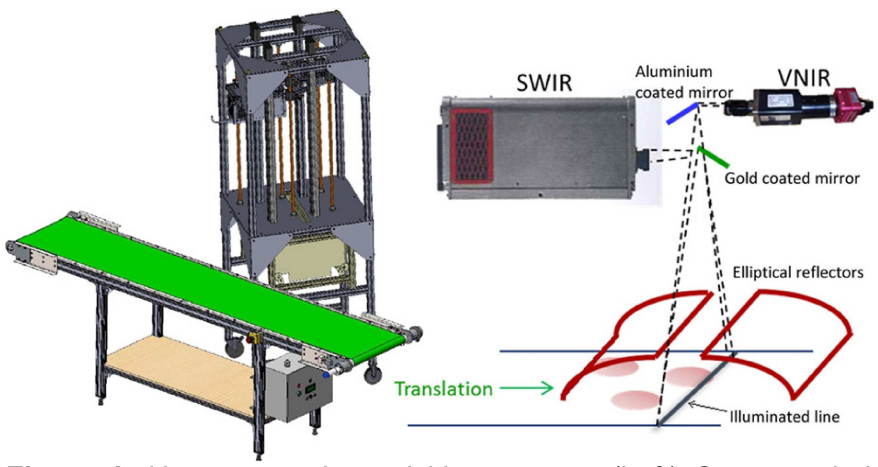

Figure 2. Hyperspectral acquisition system. (Left) Conveyor belt and metallic frame. (Right) VNIR and SWIR cameras, mirrors and illumination system with halogen lamps and extruded elliptical reflectors (Barnabé et al. 2015).

By combining data from two sensors, the result image is composed by 323 bands of 6.25 nm and digital pixels of approximately 0.25 mm². Images were spatially cropped to keep only regions of interest, avoiding long computational time. Bands up to 500 nm were considered noisy due to the high variation of pixel intensity within the spectra, which masks mineral overtones. This wavelength range was therefore removed to avoid algorithm's confusion regarding true classifications.

2.3 Spectral response

The mean spectrum of each sample was extracted from a random 20 x 20 - pixel window and plotted in a reflectance versus wavelength chart. This procedure along with False Color Composites (FCC) assisted interpretation of classification challenges to segregate rocks with similar spectral response.

Three bands were extracted from the SWIR database to highlight the presence of alteration minerals with deep absorption in the spectra. The 1940, 2200 and 2340 nm ranges were associated to the bands of an RGB image (Table 1), where reflectance is attenuated due to the presence of water, white mica and carbonate / chlorite / amphibole / white mica, respectively.

Since pixel intensity decreases in a specific wavelength interval when absorption occurs, the output represents relative concentrations where the target minerals are displayed by colors related to the opposite bands. White micas are normally concentrated in red-pinkish regions, water-rich material is represented by blue pixels and green areas are linked to carbonate / chlorite / amphibole / white mica occurrences and to the wooden box (GTK 2018 unpublished presentation). Finally, saturation and contrast were enhanced to intensify local color transitions.

Table 1. RGB bands associated to SWIR absorptions due to mineral assemblages.

RGB Band	Short Wave Infrared (nm)	Chemical group	Mineral Assemblage
R	1940	H_2O	Water
G	2200	AlOH	White Mica
B	2340	MgOH and CO_3	Carbonate/Chlorite/ Amphibole/White Mica

2.4 Supervised classification

Supervised classification was undertaken using machine learning algorithms in the perClass Library for Matlab (Fig. 3). The objective of supervised classification is to assign an image pixel to a known lithology. Dimensionality reduction with Principle Component Analysis (PCA) indicated a fall of overall performance and was initially rejected. The algorithms able to handle the dataset with satisfactory accuracy for convenient interpretation were selected: Fisher Linear Discriminant and Linear Support Vector Classifier (LSVC) (Table 2).

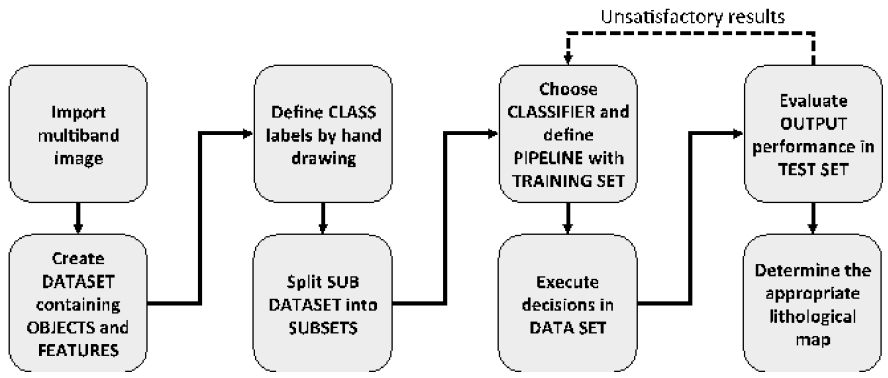

Figure 3. Scheme of supervised classification (Mendes 2018).

Table 2. Algorithms for supervised classification (Mendes 2018).

Classifier	General description
Fisher Linear Discriminant	Composed by a Linear Discrimination Analysis (LDA) component followed by a Gaussian Model
Linear Support Vector Classifier	It finds the hyperplane that separates data by classes after transforming the training set into a higher dimension.

A total of 41 classes (samples + box) are combined to test two different strategies: First, VNIR and SWIR ranges are cropped from the dataset to evaluate the performance of cameras together and individually. Subsequently, the size of training set is modified to identify the sensitiveness of classification regarding the number of labelled pixels.

The approach represents the variation of scenarios ruled by accuracy and costs.

Accuracy is computed by the mean error over classes from a confusion matrix which shows the relationship between true labels and classifier decisions.

3 Results

In general, fault rocks and bright volcanics such as dacites, breccias and tuffites show similar profile due to the presence of water and OH-bearing molecules whereas calcite veins emphasize the very deep absorptions at 2340 nm (Fig. 4). The exceptions are rocks with strong silicification such as a few tuffs and the black rhyolite. Sulphides and shales display flat curves.

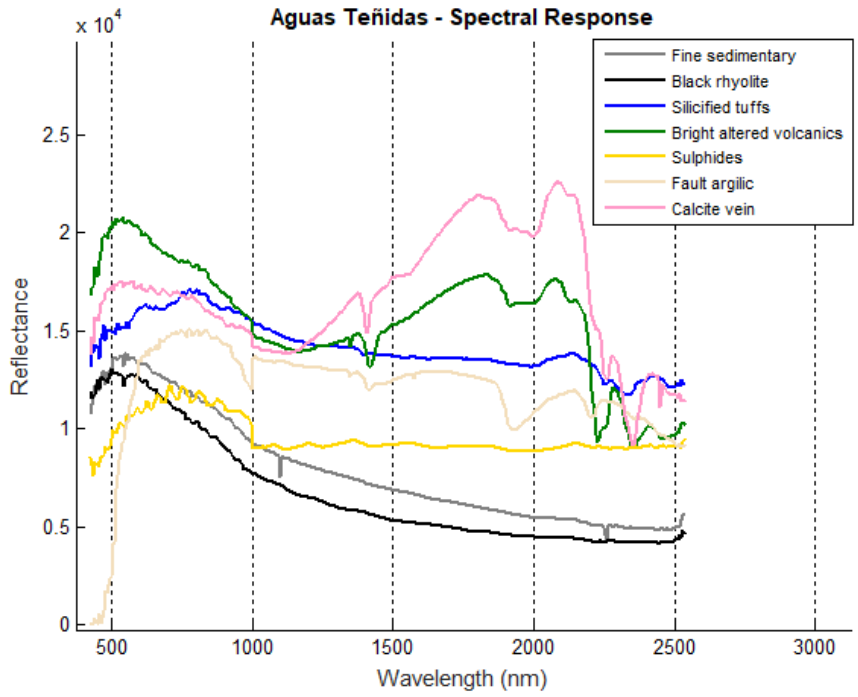

Figure 4. Spectral response of Aguas Teñidas rocks (Modified from Mendes 2018).

False Color Composites (Fig. 5) emphasize the difference between deposits of Type 1 (MAD and SOT) and Type 2 (ATE and MAG). While the latter display colourful regions, most of Type 1 samples contain dark pixels due to shales and massive/stockwork sulphides with lack of absorption features. Usually, volcanics have pink to greenish matrix where alumino-phyllosilicate-bearing zones are either intercalated or cut by thin veins of chlorite. The brightest green sample is the calcite vein located in the upper-right corner of ATE 2.

In addition, ATE 2 samples confirm an association of metal content and alteration aureoles in the Cu stockwork area of the deposit. As the segments move outwards from the mineralized zone, grey and greenish pixels are substituted by pink and reddish matrices. The network of thin veins of chalcopyrite immersed in a chloritic matrix decreases as the volume of barren sericite-rich material increases together with fine disseminated pyrite.

The supervised classification using both cameras and LSVC is the most consistent overall (Fig. 6). Average accuracy is close to 100% if LSVC is combined to many spectral bands. When only the SWIR data is used both algorithms show a slight increase in classification error. The incapability of LSVC of dealing within a small feature space is evident when only the VNIR camera is selected (78 bands). The algorithm loses almost entirely its capability of classification.

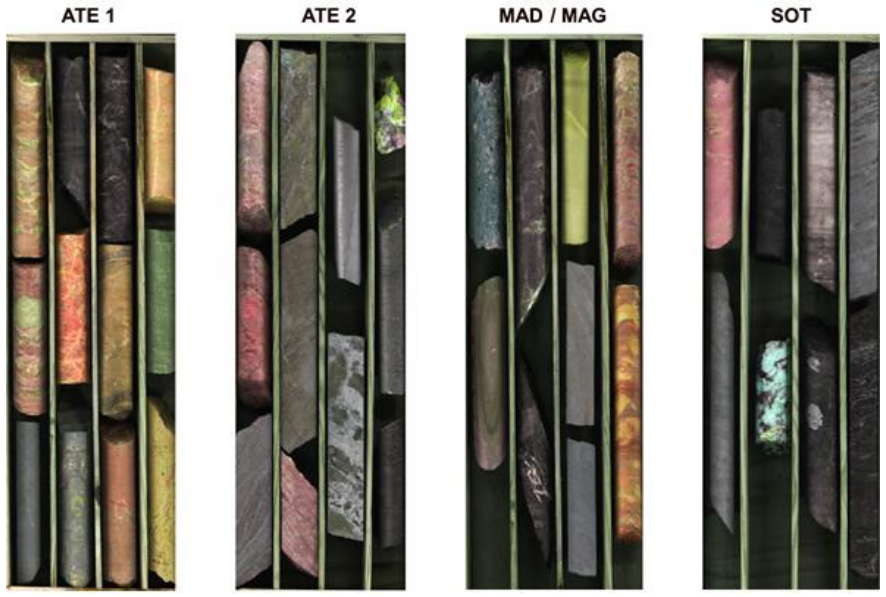

Figure 5. False color composites for alteration minerals. MAD and SOT are included in Type 1 whereas ATE and MAG are Type 2.

Another drawback of LSVC is time. The algorithm runs at low speed in most of the cases whereas decision time for Fisher is practically negligible in every scenario. Even though the accuracy of Fisher drops from almost 100% to 80% when only VNIR is used, the interpretation of images is still possible in this situation. In the case of SWIR by itself, time is the crucial parameter to elect Fisher as the best option.

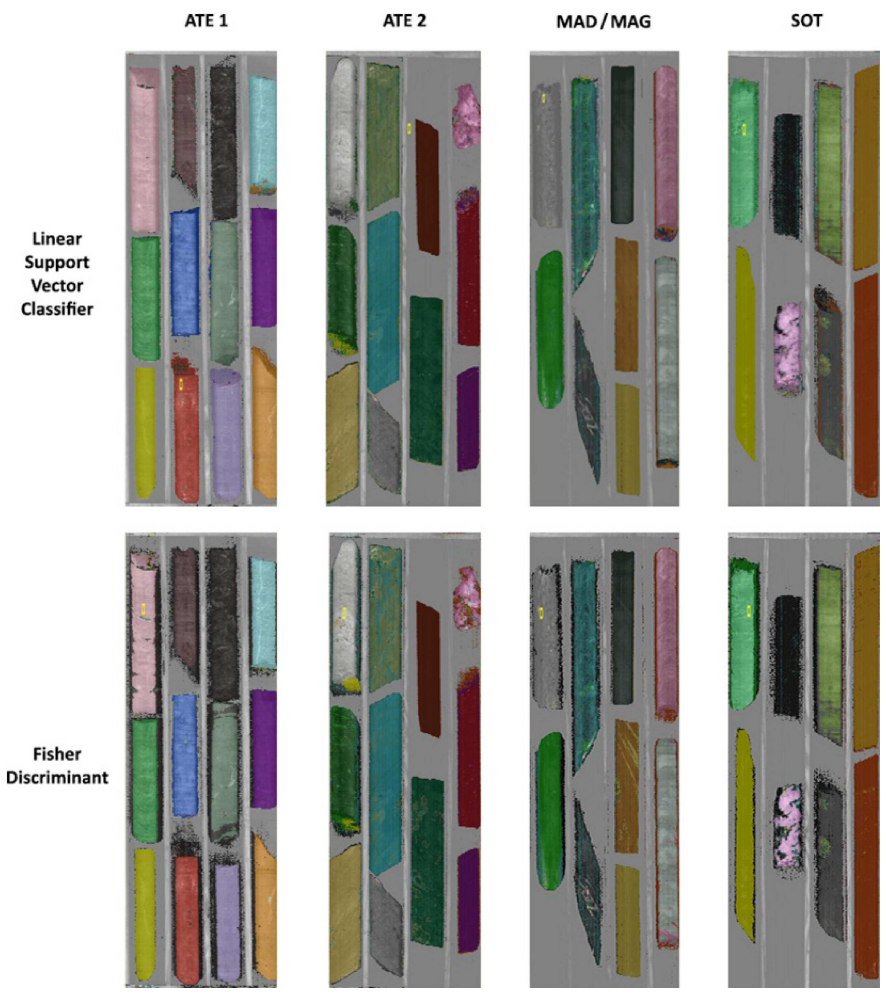

Figure 6. Most accurate classification scenario overall: VNIR-SWIR database, large training size and 41 class labels. LSVC performance is slightly more accentuated in this case. Accuracy for both type of deposits is close to 100% so that a comparison of misclassified pixels between them can be hardly evaluated through classified images (Mendes 2018).

Overall sensitiveness against training set for both classifiers is similar. However, Fisher is less accurate than LSVC at very limited subset fractions. Bearing in mind that some classes in the smallest training set (Tr4) are represented by around 5 pixels out of a test set containing 3 million pixels, the consistency of LSVC can be considered outstanding in terms of accuracy and image interpretation if applied to practical logging applications (Fig. 7).

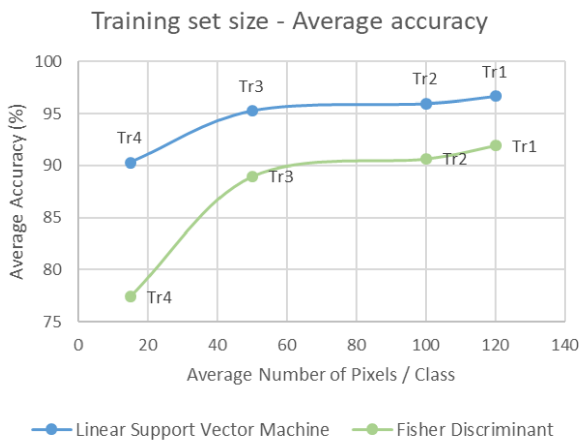

Figure 7. Accuracy with varying training set sizes (Mendes 2018).

Performance reflects the variation of absorption features in the spectra profile, being more consistent for volcanics than fine clastics in every tested scenario of classification as seen in Fig. 8.

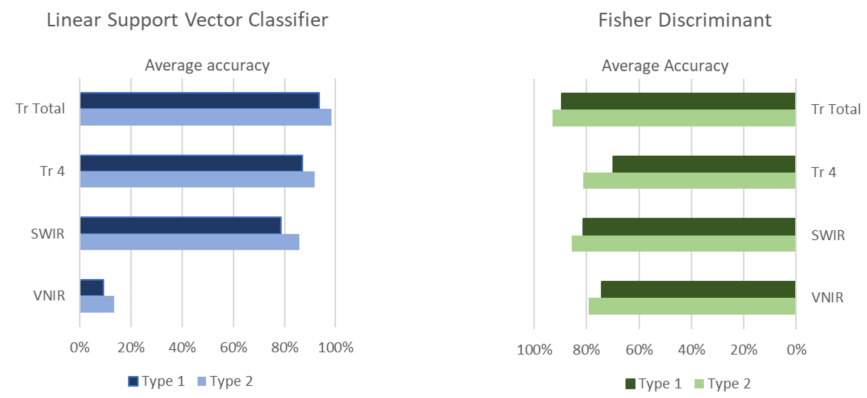

Figure 8. – Accuracy for the two deposit types (Mendes 2018).

4 Discussion

FCC and supervised classification reveal the ability of HSI to discriminate alteration degrees and rock types (Schneider et al. 2014). However, algorithms are dependent on investment in cameras and hardware.

Results demonstrate that reflectance and depth of absorption is extremely affected by grain size. Coarse material absorbs more radiation penetrating to the surface than fine grain size. The optical path is explained by the Labert-Beer Law (Zaini et al. 2012).

Since the diversity of lithologies increase in projects within time, the capability of both algorithms to deal with many classes is an advantage. Fisher is preferable over LSVC when time is crucial and when dealing with cameras independently. A significant increase in training set size can improve Fisher performance without compromising computational effort.

Areas at early exploration stages should consider a robust training set with a large number of classes from different parts of the IPB. On the other hand, drill holes from mine sites can count on a training set with restrict number of classes with only the known local lithologies.

5 Conclusion

A real performance can only be evaluated when applying decisions to complete drill cores on site. It should adapt the methodology to real geological sections where transitional contacts and textural variations are impractical to be sampled in a representative manner.

The analysis of spectral profiles with the support of FCC assists the re-construction of unbiased labels to define new logging classes. Automatization using HSI and machine learning can therefore simplify 3D models in the IPB. It can also save time and costs in projects where exploration rushes to find new deposits and to characterize the ore constantly feeding the plant.

This study successfully meets the first steps of ANCORELOG with promising business opportunities when applied to end-users such as mining companies and research institutes.

Future works should improve pixel-wise segmentation. Grades will be included through the fusion of HSI with the output of other sensors such as RGB camera, X-Ray Fluorescence (XRF), Laser Induced Breakdown Spectroscopy (LIBS) and time-gated Raman spectroscopy.

Acknowledgements

The authors would like to thank the involved team from MATSA and GeMMe for the constant support. Also, ANCORELOG partners, EMerald and EIT Raw Materials for the effort in education and research.

References

Barnabé P, Dislaire G, Leroy S, Pirard E (2015) Design and calibration of a two-camera (visible to near-infrared and short-wave infrared) hyperspectral acquisition system for the characterization of metallic alloys from the recycling industry. J Electronic Imaging 24: 61115.

Goetz, AFH, Vane G, Solomon JE, Rock BN (1985) Imaging Spectrometry for Earth Remote Sens Science 228:1147–1153.

Han J, Kamber M, Pei J (2012) Data Mining: Concepts and Techniques. Morgan Kaufmann, San Francisco

Hunt GR (1977) Spectral Signatures of Particulate Minerals in the Visible and Near Infrared. Geophysics.

Lamberg P (2012) Geometallurgy–new/old methodology to improve resource management. Materia 70:52-55.

Martin-Izard A, Arias D, Arias M, Gumiel P, Sanderson DJ, Castañon C, Sanchez J (2016) Ore deposit types and tectonic evolution of the Iberian Pyrite Belt: From transtensional basins and magmatism to transpression and inversion tectonics. Ore Geology Rev 79:254–267.

Mendes, PST (2018) Multi-sensor analysis of Aguas Teñidas, Magadalena, Sotiel and Majada deposits, Iberian Pyrite Belt, Spain: Analytical drill core-scanning for optimized exploration of ore. Dissertation, University of Liege.

Schneider S, Murphy RJ, Melkumyan A (2014) Evaluating the performance of a new classifier - the GP-OAD: A comparison with existing methods for classifying rock type and mineralogy from hyperspectral imagery. ISPRS J Photogrammetry and Remote Sens 98:145–156.

Zaini N, Van der Meer F, Van der Werff H (2012) Effect of grain size and mineral mixing on carbonate absorption features in the SWIR and TIR wavelength regions. Remote Sens 4:987-1003